Methane-Assisted Chemical Vapor Deposition Yielding Millimeter-Tall Single-Wall Carbon Nanotubes of Smaller Diameter

Zhongming Chen,[†,‡] Dong Young Kim,[‡] Kei Hasegawa,[‡] and Suguru Noda[‡,§,*]

[†]Department of Chemical System Engineering, School of Engineering, The University of Tokyo, 7-3-1 Hongo, Bunkyo-ku, Tokyo 113-8656, Japan, [‡]Department of Applied Chemistry, School of Advanced Science and Engineering, Waseda University, 3-4-1 Okubo, Shinjuku-ku, Tokyo 169-8555, Japan, and [§]PRESTO, Japan Science and Technology Agency, 4-1-8 Honcho, Kawaguchi, Saitama 332-0012, Japan

ABSTRACT We examined the use of low purity H_2 (96 vol % H_2 with 4 vol % CH_4) in chemical vapor deposition (CVD) using a C_2H_2 feedstock, and obtained vertically aligned single-wall carbon nanotubes (VA-SWCNTs) with unexpectedly smaller diameters, larger height, and higher quality compared with those grown using pure H_2. During the catalyst annealing, carbon deposited at a small amount from CH_4 on the Fe particles, which kept them small and dense. During CVD, CH_4 prevented the Fe particles from coarsening, resulting in an enhanced growth lifetime and suppressed diameter increase of growing SWCNTs. These effects were observed only for CH_4, and not for C_2H_4 or C_2H_2. CH_4-assisted CVD is an efficient and practical method that uses H_2 containing CH_4 that is available as a byproduct in chemical factories.

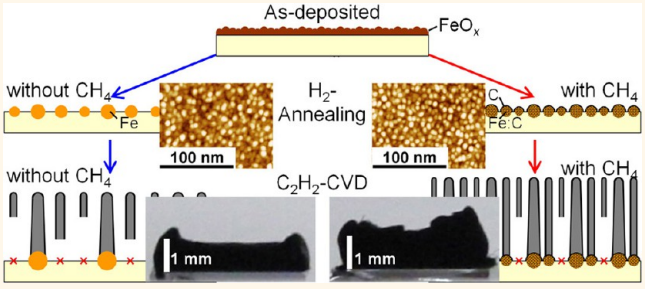

KEYWORDS: single-wall carbon nanotubes · chemical vapor deposition · H_2 annealing · Fe catalyst nanoparticles · CH_4 addition · Ostwald ripening

Growing longer carbon nanotubes (CNTs) with smaller diameters is an ever-lasting challenge. In 1996, Li *et al.* reported the synthesis of vertically aligned CNT (VA-CNT) arrays *via* chemical vapor deposition (CVD) using Fe catalysts supported on porous SiO_2.[1] These were multiwall CNTs (MWCNTs) with a diameter of ~30 nm, and their height reached 50 μm in 2 h. Later, they improved the height to 2 mm by continuing CVD for as long as 48 h.[2] For single-wall CNTs (SWCNTs), however, several more years were required for such growth to be achieved. Murakami *et al.* first realized the synthesis of VA-SWCNTs using CVD with C_2H_5OH as a feedstock, but the height was a few micrometers after 60 min of growth.[3] Hata *et al.* reported the "super growth" of VA-SWCNTs *via* water-assisted CVD; in this case, the height reached 2.5 mm in 10 min.[4] These works have driven many researchers to investigate O-containing precursors such as CO[5] in addition to C_2H_5OH,[3,6−8] and O-containing additives such as O_2,[9] CO_2,[10] and many other species[11] in addition to H_2O.[12−14] Such species can enhance the lifetime of the catalyst by removing the carbon byproducts that cover the catalyst nanoparticles.[12] Because of such efforts, it is now possible to grow millimeter-tall VA-SWCNTs; however, such SWCNTs tend to have large diameters, of ~3 nm or larger.[15−17] Catalyst nanoparticles gradually become coarsened during CVD through Ostwald ripening,[13] resulting in the abrupt termination of the growth and gradual increase in diameter of the growing SWCNTs.[14,17−19] The question of how to keep small catalyst nanoparticles stable and active for SWCNT growth is a very difficult and important issue. Increasing the length while retaining the small diameter of SWCNTs is highly demanded in applications such as transparent conducting films[20] and spun-fibers[21] where the contacts between SWCNTs limit their electrical and mechanical properties.

* Address correspondence to noda@waseda.jp.

Received for review March 29, 2013 and accepted July 11, 2013.

Published online July 11, 2013
10.1021/nn401556t

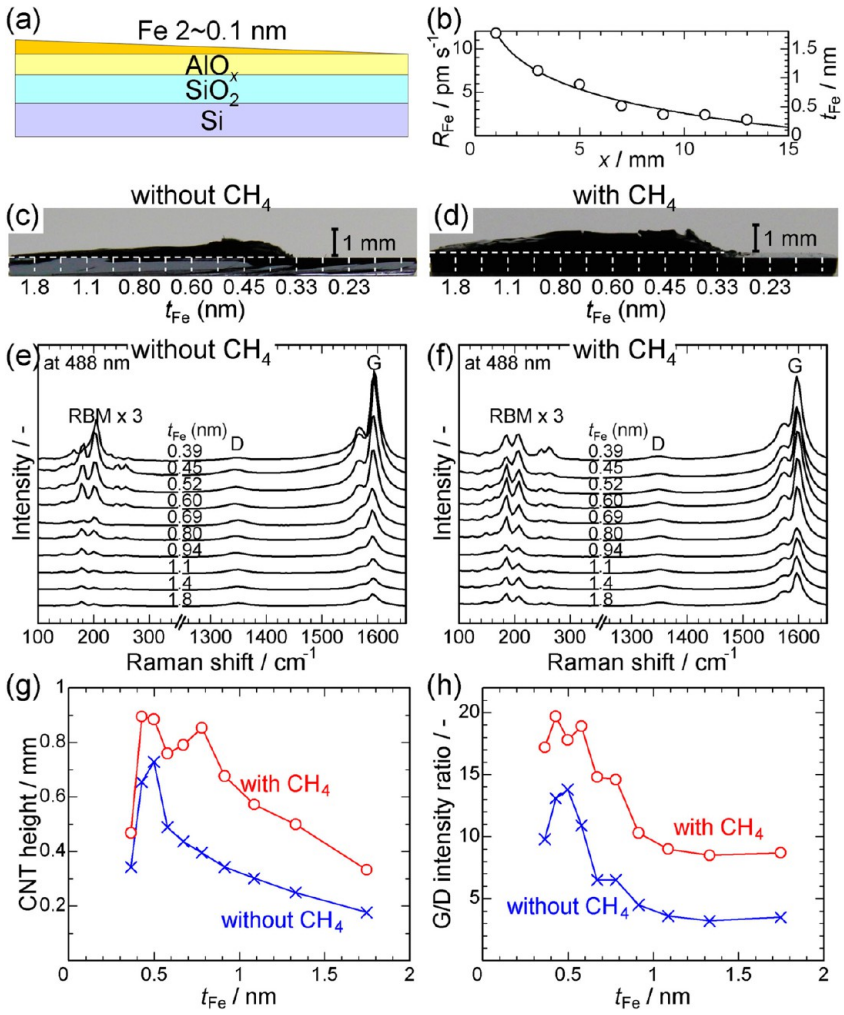

Figure 1. VA-CNTs grown on combinatorial Fe/AlO$_x$ catalyst libraries under standard conditions for 10 min without and with CH$_4$. (a) Schematic of the Fe/AlO$_x$ catalyst library. (b) Profiles of Fe deposition rate (R_{Fe}) and nominal Fe thickness (t_{Fe}) *vs* position in the library (x). Digital images (c and d) and Raman spectra (e and f) for the CNTs grown on the libraries without (c and e) and with (d and f) CH$_4$. Heights (g), and G/D intensity ratios (h) of the CNTs at different t_{Fe}. The Raman spectra were taken at the top of the VA-CNTs, using an excitation wavelength of 488 nm.

To realize the full-scale practical applications of CNTs, it is necessary to achieve low-cost and large-scale production methods. Previously, we coupled the rapid growth of VA-CNTs with the fluidized-bed CVD method to realize the semicontinuous and batch production of submillimeter-long few-wall CNTs[22] and SWCNTs,[23] respectively. The bed of catalyst-supported ceramic particles enabled the rapid conversion of C_2H_2 into CNTs with a carbon yield of ~70 at%, in residence times as short as 0.2−0.3 s. A large amount of H_2, which is a common feed gas in many CVD processes for CNT production, is needed for this process. Hence, there is a practical motivation for replacing the expensive high-purity H_2 used in laboratory processes with the low-purity H_2 that is available at a low cost and/or a byproduct in chemical factories. In the naphtha cracking process, H_2 gas is produced as a byproduct in addition to various low hydrocarbons (CH_4, C_2H_4, C_2H_6, C_3H_6, C_3H_8, *etc.*). H_2 is separated by cryogenic distillation from this mixture, but some CH_4 remains in the separated H_2. In this work, we examined the use of 96 vol % pure H_2 containing 4 vol % CH_4 for the rapid growth of millimeter-tall SWCNTs, and compared the results with those obtained using 99.999 vol %-pure H_2. We examined whether the impurity (CH_4) disturbs the SWCNT growth; unexpectedly, we found that CH_4 has significant effects in suppressing the coarsening of the catalyst particles and growing taller VA-SWCNTs with smaller diameters. We also discuss the role of CH_4 in improving the SWCNT growth.

RESULTS AND DISCUSSION

Overview of CH$_4$-Assisted CVD Yielding Taller VA-SWCNTs of Higher Quality under a Wider Range of Catalyst Conditions. Using the combinatorial masked deposition (CMD) method,[16,24,25] we could easily optimize the catalyst conditions for the SWCNT growth. Fe/AlO$_x$ catalysts with a range of nominal Fe thicknesses (t_{Fe}) were prepared by sequentially sputter-depositing Al and Fe on silicon wafers with a thermal oxide layer

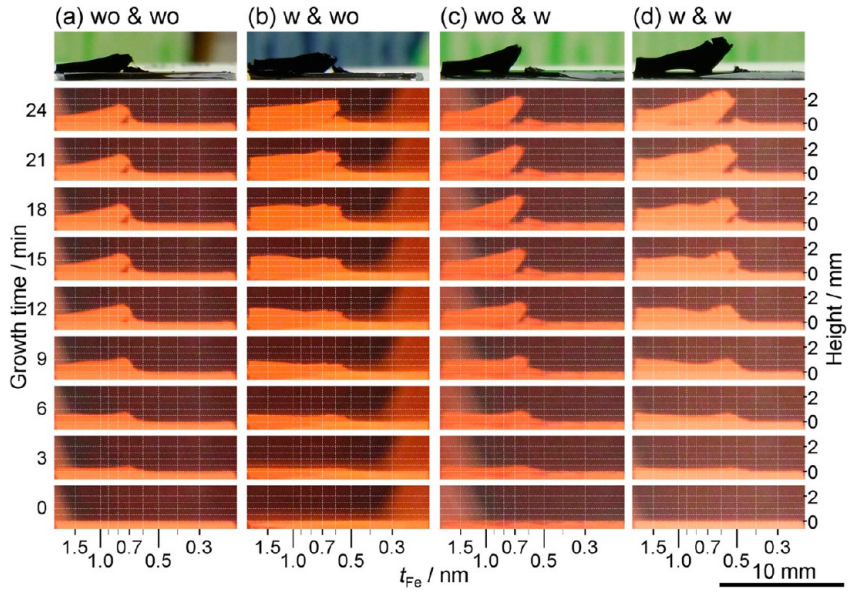

Figure 2. Photographs of the VA-CNTs taken at 3 min intervals during growth, under the conditions of: (a) annealing and CVD without CH_4, (b) annealing with CH_4 and CVD without CH_4, (c) annealing without CH_4 and CVD with CH_4, (d) annealing and CVD with CH_4. The top images were taken after the corresponding samples were cooled. The scale bar applies for all of the images.

(Figure 1a,b), and by annealing these samples in a 26 vol % H_2/Ar mixture (named here as "without CH_4"), or a 25 vol % H_2/1.0 vol% CH_4/Ar mixture (named here as "with CH_4"), both with 50 ppmv H_2O, at ambient pressure and 800 °C for 5 min in a tubular CVD reactor (see Methods). CVD was then carried out by switching the gas mixture to 0.3 vol % C_2H_2/26 vol % H_2/Ar, or 0.3 vol % C_2H_2/25 vol % H_2/1.0 vol % CH_4/Ar, both with 50 ppmv H_2O, at ambient pressure.

Figure 1c,d shows digital images of the CNTs grown on the combinatorial catalyst library using H_2/without and with CH_4, respectively. The CNTs were vertically aligned (see scanning electron microscope (SEM) images in Supporting Information, Figure S1), and their height was largely dependent on t_{Fe}, as reported previously.[14] The VA-CNTs were 0.7 mm tall at $t_{Fe} \approx$ 0.5 nm and became shorter with $t_{Fe} <$ 0.5 nm, and the CNTs hardly grew with $t_{Fe} <$ 0.3 nm (Figure 1g). The CVD conditions for Figure 1d were the same as those used for Figure 1c, except that 1.0 vol % H_2 was replaced with 1.0 vol % CH_4; however, the height of the VA-CNTs was very different. The CNTs were approximately 0.9 mm in height at $t_{Fe} \approx$ 0.5 nm and were taller than those produced without CH_4 over a wide range of t_{Fe} values (Figure 1g). Figure 1e,f shows the Raman spectra for the CNTs shown in Figure 1c,d, respectively, taken at their tops at different positions. For the VA-CNTs grown without CH_4 at $t_{Fe} \leq$ 0.6 nm (Figure 1e), the G-band peak at ≈1590 cm^{-1} was branched, and the RBM peaks appeared clearly, illustrating the growth of the SWCNTs, as we reported previously.[14,16,19] For the VA-CNTs grown with CH_4 (Figure 1d), however, the Raman spectra were quite different. The G-band peak was sharp and branched, and RBM peaks were clearly observed for a wider range of t_{Fe}, showing that the SWCNTs were synthesized under a wider range of catalyst conditions. The G-band to D-band peak intensity ratios (Figure 1h) were much larger for the CNTs grown with CH_4 than for those grown without CH_4, which indicated the higher quality of the former compared with the latter. In the following sections, we carefully examined these remarkable effects of CH_4 in enhancing the height and quality of VA-SWCNTs for $0.5 \leq t_{Fe} \leq 1$ nm; under these conditions, the SWCNTs grew to ~1 mm in height.

Effects of CH_4 during Catalyst Annealing and CVD. To investigate the effects of CH_4 during the synthesis of the SWCNTs, we used a digital camera to monitor the growth of VA-CNTs every 10 s. The photos shown in Figure 2 were taken at 3 min intervals under the conditions: (a) annealing and CVD without CH_4, (b) annealing with CH_4 and CVD without CH_4, (c) annealing without CH_4 and CVD with CH_4, and (d) annealing and CVD with CH_4. At the beginning of the CNT growth, the CNT heights were similar in all of the samples, except for the threshold in t_{Fe} for the VA-CNT growth: (a) ~0.6 nm, (b and c) ~0.5 nm, and (d) <0.5 nm (see the photos taken at 6 min). The differences in the heights became prominent in the later stages; in the final stage, the VA-CNTs were the shortest (~1.5 mm) under the (a) conditions, and the tallest (maximum height >2.5 mm) under the (d) conditions (see the photos taken after the samples were cooled). Near the threshold Fe thickness, the VA-CNTs peeled off from the substrates, due to the tension produced by the VA-CNTs growing faster and taller nearby.[14] Figure 3 shows the time profiles for the heights of the VA-CNTs at t_{Fe} = 0.7 nm. The VA-CNTs peeled off the substrate at 650−700 s with (a) and

750−800 s with (c), whereas they grew continuously for ~1300 s with (b) and ~1500 s with (d). The growth lifetime and final height were the shortest for (a) (750−800 s and 0.9 mm), and the largest for (d) (1500 s and 2.2 mm). The growth rate for (c) is somewhat larger than the others (a, b and d). As discussed later for Figure 4, annealing without CH_4 resulted in the lower density of catalyst particles, which may have resulted in the lower mass density of the CNT forests and thus the larger height increase (growth rate). But the growth curves obtained using the catalyst library is not suitable for the detailed discussion because the CNTs growing nearby at different t_{Fe} interact with each other. The addition of CH_4 during the catalyst annealing and CVD enhanced the VA-CNT height, mainly by enhancing their growth lifetime rather than the growth rate.

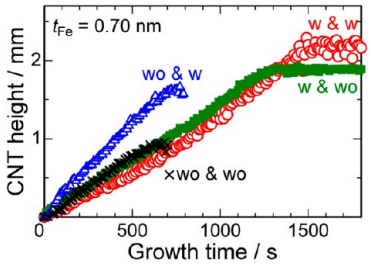

Figure 3. Time profiles of CNT heights for t_{Fe} = 0.70 nm, under the conditions of: annealing and CVD with CH_4 (red open circles), annealing with CH_4 and CVD without CH_4 (green closed squares), annealing without CH_4 and CVD with CH_4 (blue open triangles), and annealing and CVD without CH_4 (black crosses). The samples shown are the same as those shown in Figure 2.

Effects of the Addition of CH_4 during the Catalyst Annealing on the Microstructure of the Fe Particles. Figure 4 shows AFM images of the Fe/AlO_x surfaces at three different stages: as deposited (a, d, g, and j), after annealing under H_2 without CH_4 (b, e, h, and k), and after annealing under H_2 with CH_4 (c, f, i, and l). Fe was deposited uniformly on separate substrates, with different thicknesses of t_{Fe} = 1.0 nm (a−c), 0.7 nm (d−f), 0.6 nm (g−i), and 0.5 nm (j−l). The inset data shows the number density of the Fe islands or particles. The number density of the Fe particles was approximately 1.5−1.7 times higher when the samples were annealed

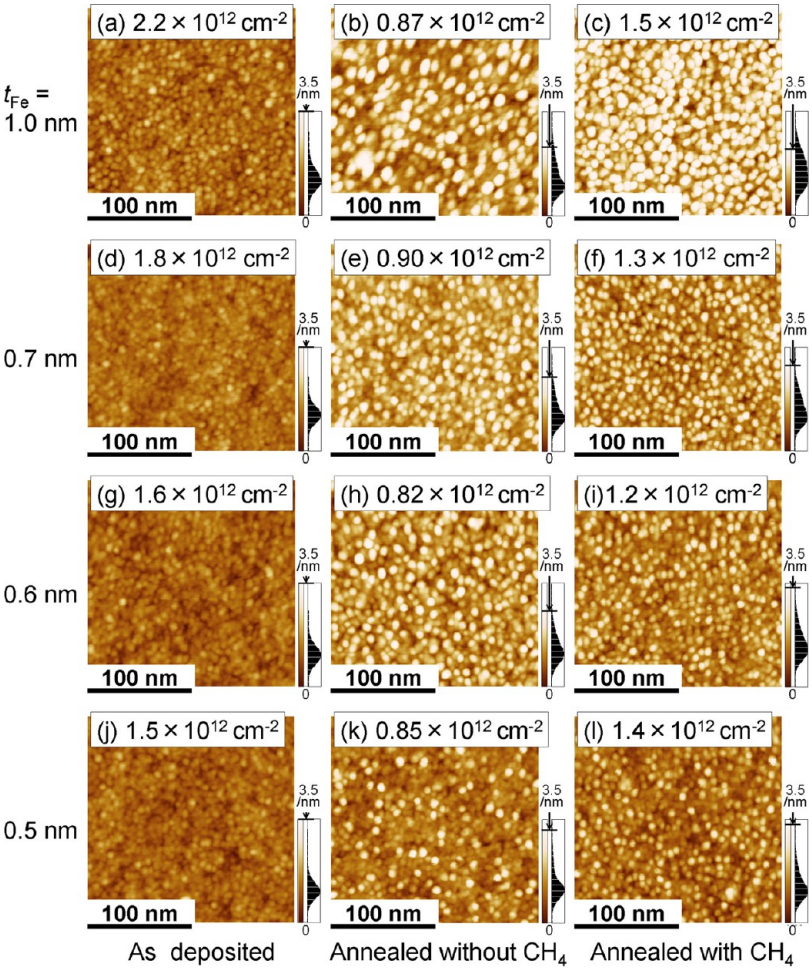

Figure 4. AFM images of the Fe/AlO_x surfaces as-deposited (a, d, g, and j), after annealing at 800 °C for 5 min under H_2/H_2O/Ar without CH_4 (b, e, h, and k), and after annealing under H_2 with CH_4 (c, f, i, and l). The catalysts were prepared on separate substrates with uniform thicknesses of t_{Fe} = 1.0 nm (a−c), 0.7 nm (d−f), 0.6 nm (g−i), and 0.5 nm (j−l). The inset show the number density of the Fe islands and particles.

under H_2 with CH_4 than when they were annealed under H_2 without CH_4. For example, nominally 0.7-nm-thick Fe formed very small islands with a number density of 1.8×10^{12} cm^{-2}, as deposited on the AlO_x surface. After annealing under H_2 without CH_4 (Figure 4e), the Fe layer transformed in particles of a larger size and a wider size distribution (see the height distribution on the right of each AFM image), and their number density decreased to 0.90×10^{12} cm^{-2}. After annealing under H_2 with CH_4 (Figure 4f), the Fe particles were small and uniform, with number densities as high as 1.3×10^{12} cm^{-2}. Similar results were found for all of the t_{Fe} in Figure 4. It is clear that CH_4 had a significant effect in keeping the Fe particles stable with small sizes and high number densities.

We then analyzed the Fe/AlO_x surfaces after annealing (and prior to CVD) using X-ray photoelectron spectroscopy (XPS) (Supporting Information, Figure S2). Although the chemical state of the Fe after annealing could not be judged from the spectra due to its oxidation during the sample transfer to the XPS chamber under air, we were able to obtain quantitative information on the surface atomic ratios. The Fe to Al atomic ratio was similar when the annealing was performed with CH_4 (0.14) and when it was performed without CH_4 (0.14). A significant difference was found in the C to Fe atomic ratio; it was 3.0 when the annealing was performed without CH_4, and it was 7.4 when the annealing was performed with CH_4. The C 1s peaks for the Fe-free AlO_x surfaces annealed without and with CH_4 exactly coincided with each other (Figure S2a), which indicates that the carbon deposited from CH_4 not on the AlO_x surface but on the Fe particles. The subtraction of the C 1s peaks for the Fe/AlO_x surfaces yielded a sharp peak centered at 284.0 eV (Figure S2b), which should reflect the carbon deposited on the Fe particles. Note that the broad peak centered at 286.1 eV that was observed for all samples originated from organic compounds adsorbed during the exposure to air. It is possible that CH_4 stabilized the Fe particles during the catalyst annealing by saturating and passivating them with carbon, thus reducing their surface energy, where the passivation layer was thin enough to allow the CNT growth in the successive CVD step and to allow the oxidation of Fe particles during their exposure to air.

Effect of the Addition of CH_4 during CVD on the Diameter of the SWCNTs. We previously observed an increase in the diameter of millimeter-tall VA-SWCNTs, from 1.5 to 2 nm at the top, to 3−4 nm at the bottom;[14,17,19] this was attributed to the coarsening of the Fe particles[14,17,19] through Ostwald ripening[13] during CVD. The coarsening of the catalyst is also closely related to the termination of CNT growth.[18,26] Because there is a close relationship between the diameter of the catalyst particles and that of the SWCNTs,[27,28] the change in the diameter of the SWCNTs at different positions along their height should reflect the history of the change in the diameter of the catalyst particles during CVD. We therefore analyzed the SWCNTs in detail using transmission electron microscopy (TEM).

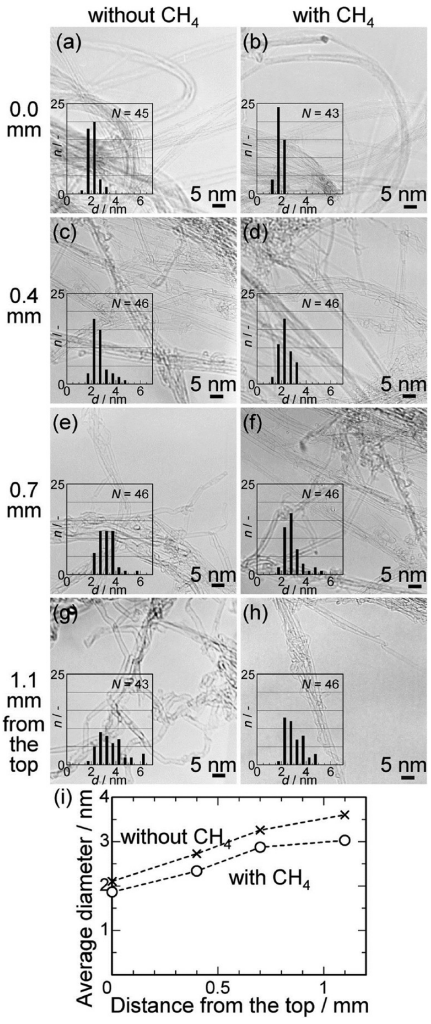

Figure 5. TEM images and diameter distributions of SWCNTs, observed at different depths from the top of the VA-SWCNTs. The SWCNTs were grown for 10 min on separate substrates with a uniform catalyst of t_{Fe} = 0.7 nm, without (a, c, e, and g) and with (b, d, f, and h) the addition of CH_4 throughout catalyst annealing and CVD (also see Supporting Information, Figure S1). The change in the average diameter of the SWCNTs was plotted against the depth from the top of the VA-SWCNTs in (i).

We synthesized VA-SWCNTs on separate substrates with a uniform catalyst of t_{Fe} = 0.7 nm, without and with CH_4 throughout catalyst annealing and CVD. As shown in Supporting Information Figure S1, the SWCNTs were vertically aligned, and were taller when CH_4 was added. The Raman spectra and the G-band to D-band intensity ratios confirmed that the SWCNTs were of better quality when CH_4 was added, which was consistent with the results shown in Figure 1. A portion

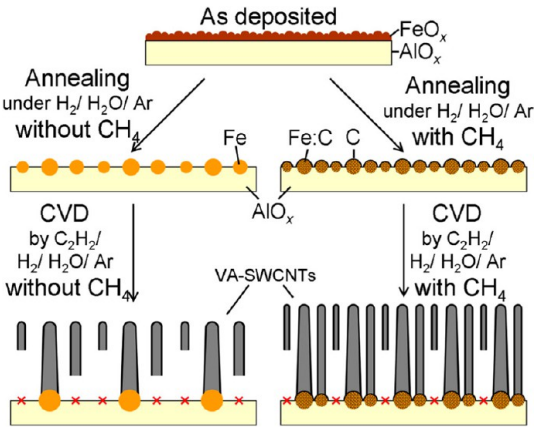

Figure 6. Schematic representation of the catalyst annealing and CVD growth of VA-SWCNTs, without and with CH_4.

of the VA-SWCNTs was picked up using tweezers, laid on a TEM grid, and observed (using TEM) at various depths from the top of the VA-SWCNTs (Figure 5).[17] All of the CNTs were SWCNTs, and no MWCNTs were observed at any depths, similar to our previous reports.[14,17,19] The inset histograms for the SWCNT diameter distributions showed that the diameter was smaller when the synthesis was performed with CH_4, and that it increased with increasing depth. Figure 5i shows the average diameter of the SWCNTs at different depths from the top of the VA-SWCNTs. The diameter increased from 2.1 to 3.6 nm in the case without CH_4 addition, while it increased from 1.9 to 3.0 with CH_4 addition. Because SWCNTs grow in the root growth mode, this result shows that the diameter of SWCNTs increased with time during CVD. Although the SWCNTs increased in diameter regardless of the addition of CH_4, SWCNTs with smaller diameters nucleated and grew from the smaller catalyst particles (Figure 4), and retained their smaller diameters when CVD was performed with the addition of CH_4. CH_4 suppressed the coarsening of the catalyst to some extent, during both the catalyst annealing and the CVD, yielding taller VA-SWCNTs (Figure 1 and S1) with smaller diameters (Figure 5).

Possible Role of CH_4 during Catalyst Annealing and during CVD. Figure 6 summarizes the possible role of CH_4 during the catalyst annealing and the CVD growth of the VA-SWCNTs. After sputter-deposition and exposure to air, the Fe was in an oxidized state, and had a very fine particulate island structure (Figure 4a,d,g,j). When annealed under H_2 without CH_4, the increased surface energy of the reduced Fe drove the coarsening of the Fe particles, resulting in larger Fe particles and reduced number densities (Figure 4b,e,h,k). In contrast, when the annealing was performed under H_2 with CH_4, carbon deposited at a small amount (Figure S2a), which possibly saturated Fe particles and passivated their surface, reducing their surface energy and thus suppressing the driving force for the coarsening process, resulting in small Fe particles with high number densities (Figure 4c,f,i,l). However, CH_4 neither deactivated the catalyst particles by forming "onions", nor grew CNTs under our experimental conditions. The reactivity of CH_4, which is much smaller than that of C_2H_2,[29] should have been sufficient to just stabilize small Fe particles. The addition of CH_4 was also effective in the subsequent CVD step, in allowing the SWCNTs to grow taller (Figure 3), and in suppressing increases in the diameter of the growing SWCNTs (Figure 5). Such effects can be understood in a fashion similar to the annealing step; *i.e.*, CH_4 stabilized the small Fe particles, and prevented them from coarsening through Ostwald ripening. Although we did not observe the mass loss of Fe through the subsurface diffusion to the AlO_x underlayer, which reportedly occurs at the later stage than Ostwald ripening,[30] CH_4 may show some effect in suppressing the mass loss, too, for the case of longer CVD time. The question remains as to why CH_4 was needed during CVD, because there was a much larger influx of carbon from the C_2H_2 (millimeter length corresponding to $10^{6\sim7}$ layers) than from the CH_4 (up to a few layers).

Effects of Other Hydrocarbons: Catalyst Annealing under H_2 with CH_4, C_2H_4, and C_2H_2. We next examined the addition of C_2H_2 and C_2H_4, which are popular and efficient carbon feedstocks for SWCNTs, during "catalyst annealing", *i.e.*, during heating to and holding for 5 min at 800 °C, and compared their effects with that of CH_4. Figure 7a,c,g shows photographs of the Fe/AlO_x surfaces (t_{Fe} = 0.70 nm) after "annealing" under H_2 with CH_4, C_2H_4, and C_2H_2, respectively. No CNTs grew with the addition of CH_4 (Figure 7a,b) and only catalyst annealing took place. Irregularly big particles were observed at a very low density on the substrate surface (Figure 7b). Note that the resolution of the SEM was insufficient to observe the tiny particles observed by AFM (Figure 4). When C_2H_4 was added, not only the catalyst annealing but also CVD took place and 0.1-mm-tall VA-CNTs grew uniformly on the substrate (Figure 7c−f). The CNTs were well aligned vertically, and their Raman spectrum (Figure 9a) showed a branched G-band peak with a RBM peak, which are characteristic for SWCNTs. Their G/D ratio of 5.7 was similar to that of SWCNTs grown using C_2H_2, without the addition of CH_4 (Figure 1e,h); this indicated that C_2H_4 played a role as a carbon feedstock, but did not play a role in keeping the Fe particles small and dense. Note that C_2H_4 pyrolyzes and yields C_2H_2 under our experimental conditions (a residence time of 4 s at 800 °C),[31] resulting a CNT growth from C_2H_4[16−18] that was similar to that from C_2H_2.[14,19] With the addition of C_2H_2, the catalyst annealing as well as CVD took place, however, the CNTs grew only over a part of the substrate in a dotted pattern (Figure 7h). In their Raman spectrum (Figure 9b), the G-band peak was

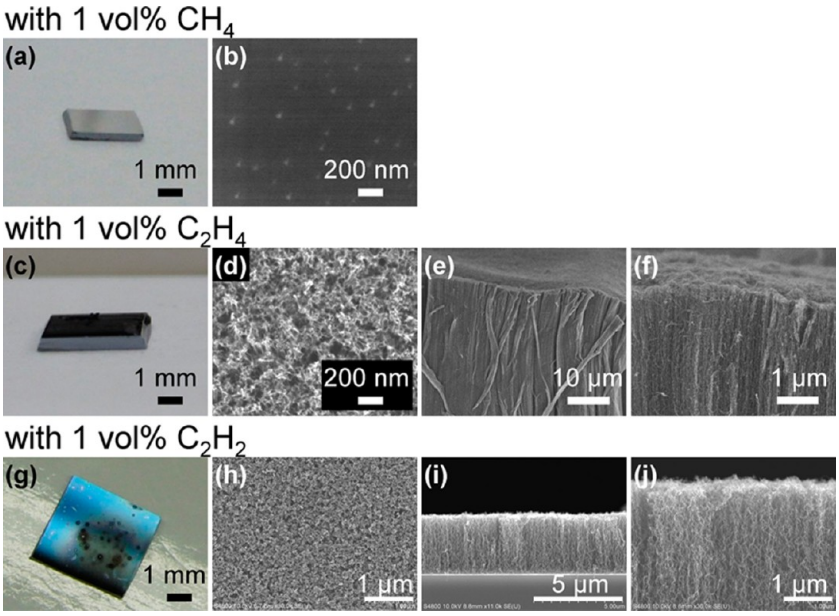

Figure 7. Photographs (a, c, and g), top-view SEM images (b, d, and h), and cross-sectional SEM images (e, f, i, and j) of the Fe/AlO_x surfaces (t_{Fe} = 0.70 nm) after "annealing" (*i.e.*, heating to and holding for 5 min at 800 °C) under 25 vol % H_2/50 ppmv H_2O/Ar with 1 vol % CH_4 (a and b), 1 vol % C_2H_4 (c–f), and 1 vol % C_2H_2 (g–j). No CNTs grew with the addition of CH_4 (a), VA-CNTs grew uniformly with the addition of C_2H_4 (c), and VA-CNTs grew in a small part of the substrate with the addition of C_2H_2 (g). SEM images (h–j) were taken at the black dotted patterns in (g).

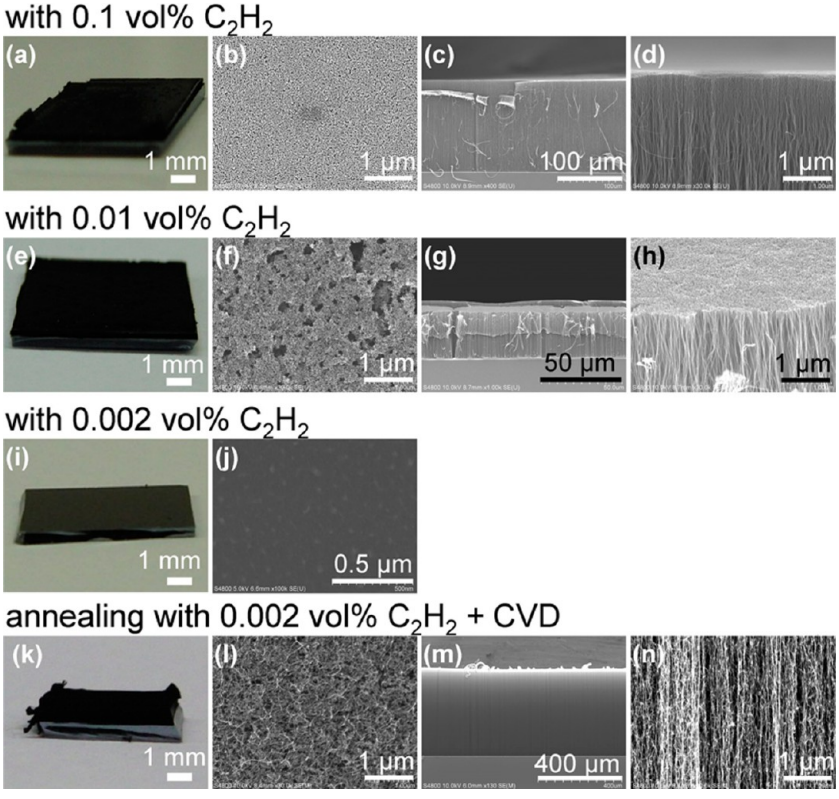

Figure 8. Photographs (a, e, i, and k), top-view SEM images (b, f, j, and l), and cross-sectional SEM images (c, d, g, h, m, and n) of the Fe/AlO_x surfaces (t_{Fe} = 0.70 nm) after "annealing" (heating to and holding for 5 min at 800 °C) under 26 vol % H_2/50 ppmv H_2O/Ar with C_2H_2 of 0.1 (a–d), 0.01 (e–h), and 0.002 vol % (i, j, amd k–n). For (k–n), CVD was also done with 0.302 vol % C_2H_2/26 vol % H_2/50 ppmv H_2O/Ar at 800 °C for 10 min after annealing.

broad, the RBM peaks were absent, and the G/D intensity ratio was as small as 0.96, indicating the formation of low-quality MWCNTs. These results show that CH_4, which has the lowest reactivity,[29] was effective in forming small and densely packed Fe particles that resulted in tall VA-SWCNTs with small diameters; C_2H_4, which

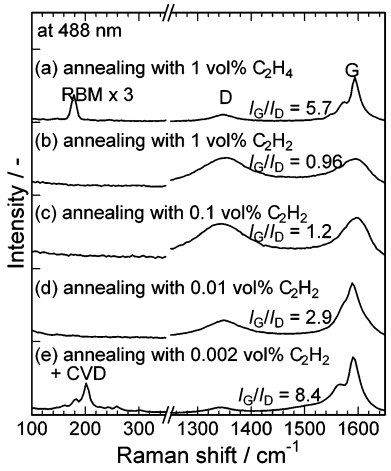

Figure 9. Raman spectra for the Fe/AlO_x surfaces with t_{Fe} = 0.70 nm after "annealing" (heating to and holding for 5 min at 800 °C) under 25 vol % H_2/50 ppmv H_2O/Ar with either (a) 1 vol % C_2H_4 or (b) 1 vol % C_2H_2, and under 26 vol % H_2/50 ppmv H_2O/Ar with (c) 0.1 vol % C_2H_2 and (d) 0.01 vol % C_2H_2. For (e), the sample was "annealed" under 26 vol % H_2/50 ppmv H_2O/Ar with 0.002 vol % C_2H_2 and then CVD was done with 0.302 vol % C_2H_2/26 vol% H_2/ 50 ppmv H_2O/Ar at 800 °C for 10 min. The samples were the same as those shown in Figure 7c–f (a), 7g–j (b), 8a–d (c), 8e–h (d), and 8k–n (e).

has a moderate reactivity,[29] had no significant effect on the stability of the Fe particles, and functioned as a feedstock for the VA-SWCNTs; and C_2H_2, which has the highest reactivity,[29] deactivated the small Fe particles and yielded MWCNTs during the annealing step (*i.e.*, heating the sample to and holding it at 800 °C under an H_2 environment).

Here arises a question: which are important, the reactivity of the hydrocarbon additives or the carbon deposition rate? We then studied the effect of the C_2H_2 addition for a range of its concentration. With 0.1 and 0.01 vol % C_2H_2, VA-CNTs grew uniformly over the substrate (Figure 8a–h). In their Raman spectra (Figure 9c,d), however, the G-band peak was broad, the RBM peaks were absent, and the G/D intensity ratio was as small as 1.2 and 2.9, respectively, indicating the formation of low-quality MWCNTs. Further decrease in C_2H_2 concentration to 0.002 vol % resulted in no CNT growth (Figure 8i,j), and only the irregularly big particles at a very low density were observed in the top-view SEM image. Because this result with 0.002 vol % C_2H_2 was similar with that with 1 vol % CH_4, we examined CVD using this catalyst. We first "annealed" the Fe/AlO_x sample under 26 vol % H_2/50 ppmv H_2O/Ar with 0.002 vol % C_2H_2 and then carried out CVD with 0.302 vol % C_2H_2 with 26 vol % H_2/50 ppmv H_2O/Ar at 800 °C for 10 min, mimicking the condition "with CH_4 throughout" but replacing 1 vol % CH_4 with 0.002 vol % C_2H_2 and 1 vol % H_2. VA-CNTs grew uniformly over the substrate (Figure 8k–n) and had a height of 0.40 mm and G/D ratio of 8.4. Compared with the VA-SWCNTs grown "without CH_4 throughout" having a height of ~1 mm and G/D ratio of 5.4 (Figure S1), the height was smaller and the G/D ratio was larger. Compared with the VA-SWCNTs grown "with CH_4 throughout" having a height of >1 mm and G/D ratio of 12.6 (Figure S1), both the height and G/D ratio were smaller. It was very difficult to achieve the similar effect of 1 vol% CH_4 by adjusting the C_2H_2 concentration. We conclude that CH_4 having a low reactivity is effective in forming small and densely packed Fe particles and growing tall VA-SWCNTs with small diameters.

CONCLUSIONS

In summary, we found that the addition of CH_4 in both the annealing and CVD steps is effective in keeping the Fe particles small and dense, and yielding taller VA-SWCNTs with smaller diameters. During the catalyst annealing, the CH_4 deposited carbon at a small amount on the Fe particles, which prevented the coarsening of the Fe particles through Ostwald ripening, possibly by reducing the surface energy of the Fe particles. CH_4 also prevented the coarsening of the Fe particles during CVD, enhancing the growth lifetime and preventing increases in the diameter of the VA-SWCNTs. Further study is needed to clarify the role of CH_4, because there was a huge influx of carbon to the Fe particles from C_2H_2 during CVD. These effects of CH_4 widened the window of catalyst conditions suitable for the rapid growth of VA-SWCNTs. When C_2H_4 (which has a moderate reactivity) was added during the catalyst annealing, it functioned only as a feedstock for CVD, yielding VA-SWCNTs without improving the quality of the SWCNTs. When C_2H_2 (which has a high reactivity) was added during the catalyst annealing, it deactivated the small catalyst particles and yielded nonuniform VA-MWCNTs. CH_4-assisted CVD is an efficient and practical method that uses H_2 containing CH_4, which is available as a byproduct in chemical factories.

METHODS

The SWCNT growth process has been described in detail elsewhere.[14,16,19] Briefly, the catalysts were prepared on silicon wafers with a thermal oxide layer. First, the substrate surfaces were pretreated by dipping them into a mixed solution of H_2SO_4 (98 wt %) and H_2O_2 (30 wt %) (with a volume ratio of 3:1) for 5 min, followed by washing with deionized water. A 15-nm-thick Al layer was then sputter-deposited on the substrate, and partially oxidized *via* exposure to air. Finally, Fe catalysts were sputter-deposited on the Al layer, either with a uniform thickness of 0.5, 0.6, 0.7, or 1.0 nm, or with a gradient thickness profile of 0.1–2 nm; this was achieved using our previously described CMD method, in which the deposition flux distribution was formed by a physical filter during the sputter deposition.[24,25] The substrate with the catalysts was placed in a tubular CVD reactor (34 mm inner diameter and 300 mm heating zone

length) and annealed during heating to and holding for 5 min at 800 °C, under a gas flow of 26 vol % H_2/50 ppmv H_2O/Ar, or 25 vol % H_2/1 vol % CH_4/50 ppmv H_2O/Ar, at ambient pressure. During this heat treatment, the Fe formed nanoparticles of a certain diameter and number density, depending on the initial Fe thickness. CVD was then carried out by adding C_2H_2 to the gas. The standard CVD conditions were either 0.3 vol % C_2H_2/26 vol % H_2/50 ppmv H_2O/Ar (without CH_4), or 0.3 vol % C_2H_2/25 vol % H_2/1 vol % CH_4/50 ppmv H_2O/Ar (with CH_4), both fed at a flow rate of 500 sccm, at ambient pressure. The samples were monitored during CVD using a digital camera to obtain side-view images every 10 s, through a window on one side of the reaction tube. The spacial resolution was 0.03 mm per pixel. The catalyst particles were analyzed after annealing using AFM (Shimadzu SPM-9600), and XPS (JEOL JPS-9010TR) with a monochromatized Mg Kα X-ray source. After CVD, the resulting CNTs were analyzed using SEM (Hitachi S-4800), Raman scattering spectroscopy (Horiba HR800), and TEM (JEOL 2000EX). The TEM samples were prepared by picking up a portion of the VA-SWCNTs and laying it on a TEM grid using tweezers.[17]

Conflict of Interest: The authors declare no competing financial interest.

Acknowledgment. This work was financially supported by Hitachi Chemical Co. Ltd., Kakenhi (Nos. 19054003, and 21686074) from MEXT, Japan, by PRESTO (No. 3130) from JST, Japan, and by ALCA from JST, Japan. We thank T. Ito for assistance in the TEM observations. The TEM observations were conducted at the Center for Nano Lithography and Analysis, The University of Tokyo. Z.C. was supported by the Scholarship under the State Scholarship Fund by the China Scholarship Council (CSC) and the Global COE Program for Mechanical Systems Innovation.

Supporting Information Available: The photographs and SEM images for SWCNT arrays synthesized without and with CH_4 addition and the corresponding Raman spectra; XPS spectra for the AlO_x and Fe/AlO_x surfaces after reduction by H_2/ H_2O/Ar without and with CH_4. This material is available free of charge *via* the Internet at http://pubs.acs.org.

REFERENCES AND NOTES

1. Li, W. Z.; Xie, S. S.; Qian, L. X.; Chang, B. H.; Zou, B. S.; Zhou, W. Y.; Zhao, R. A.; Wang, G. Large-Scale Synthesis of Aligned Carbon Nanotubes. *Science* **1996**, *274*, 1701–1703.
2. Pan, Z. W.; Xie, S. S.; Chang, B. H.; Wang, C. Y.; Lu, L.; Liu, W.; Zhou, W. Y.; Li, W. Z.; Qian, L. X. Very Long Carbon Nanotubes. *Nature* **1998**, *394*, 631–632.
3. Murakami, Y.; Chiashi, S.; Miyauchi, Y.; Hu, M.; Ogura, M.; Okubo, T.; Maruyama, S. Growth of Vertically Aligned Single-Walled Carbon Nanotube Films on Quartz Substrates and Their Optical Anisotropy. *Chem. Phys. Lett.* **2004**, *385*, 298–303.
4. Hata, K.; Futaba, D. N.; Mizuno, K.; Namai, T.; Yumura, M.; Iijima, S. Water-Assisted Highly Efficient Synthesis of Impurity-Free Single-Walled Carbon Nanotubes. *Science* **2004**, *306*, 1362–1364.
5. Zhang, L.; Tan, Y. Q.; Resasco, D. E. Controlling the Growth of Vertically Oriented Single-Walled Carbon Nanotubes by Varying the Density of Co-Mo Catalyst Particles. *Chem. Phys. Lett.* **2006**, *422*, 198–203.
6. Ohno, H.; Takagi, D.; Yamada, K.; Chiashi, S.; Tokura, A.; Homma, Y. Growth of Vertically Aligned Single-Walled Carbon Nanotubes on Alumina and Sapphire Substrates. *Jpn. J. Appl. Phys.* **2008**, *47*, 1956–1960.
7. Sugime, H.; Noda, S. Millimeter-Tall Single-Walled Carbon Nanotube Forests Grown from Ethanol. *Carbon* **2010**, *48*, 2203–2211.
8. Sugime, H.; Noda, S. Cold-Gas Chemical Vapor Deposition to Identify the Key Precursor for Rapidly Growing Vertically-Aligned Single-Wall and Few-Wall Carbon Nanotubes from Pyrolyzed Ethanol. *Carbon* **2012**, *50*, 2953–2960.
9. Zhang, G. G.; Mann, D.; Zhang, L.; Javey, A.; Li, Y. M.; Yenilmez, E.; Wang, Q.; McVittie, J. P.; Nishi, Y.; Gibbons, J.; *et al.* Ultra-High-Yield Growth of Vertical Single-Walled Carbon Nanotubes: Hidden Roles of Hydrogen and Oxygen. *Proc. Natl. Acad. Sci. U.S.A.* **2005**, *102*, 16141–16145.
10. Wen, Q.; Qian, W. Z.; Wei, F.; Liu, Y.; Ning, G. Q.; Zhang, Q. CO_2-Assisted SWNT Growth on Porous Catalysts. *Chem. Mater.* **2007**, *19*, 1226–1230.
11. Futaba, D. N.; Goto, J.; Yasuda, S.; Yamada, T.; Yumura, M.; Hata, K. General Rules Governing the Highly Efficient Growth of Carbon Nanotubes. *Adv. Mater.* **2009**, *21*, 4811–4815.
12. Yamada, T.; Maigne, A.; Yudasaka, M.; Mizuno, K.; Futaba, D. N.; Yumura, M.; Iijima, S.; Hata, K. Revealing the Secret of Water-Assisted Carbon Nanotube Synthesis by Microscopic Observation of the Interaction of Water on the Catalysts. *Nano Lett.* **2008**, *8*, 4288–4292.
13. Amama, P. B.; Pint, C. L.; McJilton, L.; Kim, S. M.; Stach, E. A.; Murray, P. T.; Hauge, R. H.; Maruyama, B. Role of Water in Super Growth of Single-Walled Carbon Nanotube Carpets. *Nano Lett.* **2009**, *9*, 44–50.
14. Hasegawa, K.; Noda, S. Millimeter-Tall Single-Walled Carbon Nanotubes Rapidly Grown with and without Water. *ACS Nano* **2011**, *5*, 975–984.
15. Yamada, T.; Namai, T.; Hata, K.; Futaba, D. N.; Mizuno, K.; Fan, J.; Yudasaka, M.; Yumura, M.; Iijima, S. Size-Selective Growth of Double-Walled Carbon Nanotube Forests from Engineered Iron Catalysts. *Nat. Nanotechnol.* **2006**, *1*, 131–136.
16. Noda, S.; Hasegawa, K.; Sugime, H.; Kakehi, K.; Zhang, Z.; Maruyama, S.; Yamaguchi, Y. Millimeter-Thick Single-Walled Carbon Nanotube Forests: Hidden Role of Catalyst Support. *Jpn. J. App. Phys.* **2007**, *46*, L399–L401.
17. Hasegawa, K.; Noda, S. Diameter Increase in Millimeter-Tall Vertically Aligned Single-Walled Carbon Nanotubes during Growth. *Appl. Phys. Express* **2010**, *3*, 045103.
18. Hasegawa, K.; Noda, S. Real-Time Monitoring of Millimeter-Tall Vertically Aligned Single-Walled Carbon Nanotube Growth on Combinatorial Catalyst Library. *Jpn. J. Appl. Phys.* **2010**, *49*, 085104.
19. Hasegawa, K.; Noda, S. Moderating Carbon Supply and Suppressing Ostwald Ripening of Catalyst Particles to Produce 4.5-mm-Tall Single-Walled Carbon Nanotube Forests. *Carbon* **2011**, *49*, 4497–4504.
20. Kaskela, A.; Nasibulin, A. G.; Timmermans, M. Y.; Aitchison, B.; Papadimitratos, A.; Tian, Y.; Zhu, Z.; Jiang, H.; Brown, D. P.; Zakhidov, A.; *et al.* Aerosol-Synthesized SWCNT Networks with Tunable Conductivity and Transparency by a Dry Transfer Technique. *Nano Lett.* **2010**, *10*, 4349–4355.
21. Sundaram, R. M.; Koziol, K. K. K.; Windle, A. H. Continuous Direct Spinning of Fibers of Single-Walled Carbon Nanotubes with Metallic Chirality. *Adv. Mater.* **2011**, *23*, 5064–5068.
22. Kim, D. Y.; Sugime, H.; Hasegawa, K.; Osawa, T.; Noda, S. Sub-Millimeter-Long Carbon Nanotubes Repeatedly Grown on and Separated from Ceramic Beads in a Single Fluidized Bed Reactor. *Carbon* **2011**, *49*, 1972–1979.
23. Kim, D. Y.; Sugime, H.; Hasegawa, K.; Osawa, T.; Noda, S. Fluidized-Bed Synthesis of Sub-Millimeter-Long Single Walled Carbon Nanotube Arrays. *Carbon* **2012**, *50*, 1538–1545.
24. Noda, S.; Sugime, H.; Osawa, T.; Tsuji, Y.; Chiashi, S.; Murakami, Y.; Maruyama, S. A Simple Combinatorial Method to Discover Co-Mo Binary Catalysts that Grow Vertically Aligned Single-Walled Carbon Nanotubes. *Carbon* **2006**, *44*, 1414–1419.
25. Noda, S.; Sugime, H.; Hasegawa, K.; Kakehi, K.; Shiratori, Y. A Simple Combinatorial Method Aiding Research on Single-Walled Carbon Nanotube Growth on Substrates. *Jpn. J. Appl. Phys.* **2010**, *49*, 02BA02.
26. Meshot, E. R.; Hart, A. J. Abrupt Self-Termination of Vertically Aligned Carbon Nanotube Growth. *Appl. Phys. Lett.* **2008**, *92*, 113107.

27. Cheung, C. L.; Kurtz, A.; Park, H. K.; Lieber, C. M. Diameter-Controlled Synthesis of Carbon Nanotubes. *J. Phys. Chem. B* **2002**, *106*, 2429–2433.
28. Nasibulin, A. G.; Pikhitsa, P. V.; Jiang, H.; Kauppinen, E. I. Correlation between Catalyst Particle and Single-Walled Carbon Nanotube Diameters. *Carbon* **2005**, *43*, 2251–2257.
29. Eres, G.; Kinkhabwala, A. A.; Cui, H. T.; Geohegan, D. B.; Puretzky, A. A.; Lowndes, D. H. Molecular Beam-Controlled Nucleation and Growth of Vertically Aligned Single-Wall Carbon Nanotube Arrays. *J. Phys. Chem. B* **2005**, *109*, 16684.
30. Kim, S. M.; Pint, C. L.; Amama, P. B.; Zakharov, D. N.; Hauge, R. H.; Maruyama, B.; Stach, E. A. Evolution in Catalyst Morphology Leads to Carbon Nanotube Growth Termination. *J. Phys. Chem. Lett.* **2010**, *1*, 918–922.
31. Itoh, R.; Noda, S.; Osawa, T.; Maruyama, S.; Yamaguchi, Y. Crucial Role of Ethylene Pyrolysis in Millimeter Growth of Single-Walled Carbon Nanotubes as Evidenced by Separate Optimization of Gas and Catalyst Temperatures, Presented at the 2008 MRS Spring Meeting, San Francisco, CA, March 2008; P4.26.